CMS Physics Analysis Summary

Contact: cms-pag-conveners-susy@cern.ch 2015/04/16

Search for supersymmetry in events with soft leptons, low jet multiplicity, and missing transverse momentum in proton-proton collisions at $\sqrt{s} = 8$ TeV

The CMS Collaboration

Abstract

A search for supersymmetry with a compressed mass spectrum is presented. Events are selected using the presence of a high-momentum jet from initial state radiation, high missing energy, and a low-momentum muon, either as the only lepton in the event or accompanied by an electron or muon of the opposite charge. In particular, a scenario of top squark pair production is investigated, where the mass difference to the lightest supersymmetric particle (LSP) is smaller than the mass of the W boson. In this case the top squarks could undergo four-body decays to $b\ell\nu + \text{LSP}$. The search is performed in a sample of proton-proton collisions recorded with the CMS detector at a centre-of-mass energy of 8 TeV and corresponding to an integrated luminosity of 19.7 fb^{-1}. The results are consistent with the expectation from standard model processes and limits are set on the production cross section in the plane of the top squark vs. LSP masses. Assuming a 100% branching ratio of the four-body decay top squark masses below 316 GeV are excluded at 95% confidence level for a mass difference to the LSP of about 25 GeV. Results are also interpreted under the assumption of chargino-neutralino production, with subsequent decays via sleptons or sneutrinos.

1 Introduction

Among the main objectives of the physics programme at the LHC are searches for new physics, and in particular for Supersymmetry (SUSY) [1–5], one of the most promising extensions of the standard model (SM). Supersymmetric models can offer solutions to several shortcomings of the SM, in particular those related to the explanation of the mass hierarchy of elementary particles [6, 7] and to the presence of dark matter in the universe.

Supersymmetry predicts superpartners of SM particles (sparticles) whose spin differs by one-half unit with respect to their SM partners. If R-parity, a new quantum number, is conserved, SUSY particles would be pair-produced and their decay chains would end with the lightest supersymmetric particle (LSP). In many SUSY models the lightest neutralino ($\widetilde{\chi}_1^0$) takes the role of the LSP and — being neutral and weakly interacting — would match the characteristics required of a dark-matter candidate. The LSPs would remain undetected and yield a characteristic signature of high missing transverse energy ($E_{\mathrm{T}}^{\mathrm{miss}}$).

The absence of indications for SUSY in LHC data could be explained if the mass splitting between the LSP and the next-to-lightest SUSY particle(s) is small, a scenario referred to as "compressed" SUSY. It would escape classical search strategies due to the low transverse momenta (p_{T}) of the decay products. Signal events can still be distinguished from SM processes if a high-p_{T} jet from initial state radiation (ISR) leads to a boost of the sparticle pair system and enhances the amount of $E_{\mathrm{T}}^{\mathrm{miss}}$, while the other decay products would typically remain soft.

SUSY models with light top squarks ($\widetilde{\mathrm{t}}$) are well motivated since they limit the dominant correction to the Higgs boson mass and thus preserve "naturalness" [8–15]. Mass splittings of 15–30 GeV seem preferred since they would lead to the right cosmological abundance of dark matter due to $\widetilde{\mathrm{t}}$-$\widetilde{\chi}_1^0$ annihilation [16]. For mass differences below the W-boson mass top squarks could decay either via a two-body ($\widetilde{\mathrm{t}} \to \mathrm{c}\widetilde{\chi}_1^0$) or a four-body ($\widetilde{\mathrm{t}} \to \mathrm{bff}'\widetilde{\chi}_1^0$, where ff′ represents a pair of quarks or leptons) decay with branching ratios depending on details of the model. The search strategy based on the presence of an ISR jet has been used to search for the two-body decay in a monojet topology by CMS [17], and for both decay modes by ATLAS [18, 19].

In this Letter we describe a search for $\widetilde{\mathrm{t}}\widetilde{\mathrm{t}}$ production with subsequent four-body decays in events with a high-p_{T} jet, $E_{\mathrm{T}}^{\mathrm{miss}}$, and one or two soft leptons, corresponding to signal events with a leptonic decay of at least one of the virtual W bosons. The single-lepton topology offers the second-highest branching ratio after the purely hadronic mode. In this channel we consider only muons, which can be efficiently reconstructed and identified with transverse momenta as low as 5 GeV. For the dilepton topology we additionally require a second lepton (electron or muon) of opposite charge. In addition events are selected including a high-momentum jet compatible with the ISR signature, at most one additional jet of moderate to high p_{T}, no hard leptons, and a significant amount of $E_{\mathrm{T}}^{\mathrm{miss}}$. The dominant SM backgrounds to this search are pair production of top quarks, W boson or Z/γ^* production in association with jets, and diboson (VV) production. Their contributions to the signal region are estimated by correcting the predictions from simulation based on several control regions in data. Data is also used to validate this procedure and to derive systematic uncertainties.

The results of the dilepton search are also interpreted in a model of pair production of the lightest chargino ($\widetilde{\chi}_1^+$) with the second-lightest neutralino ($\widetilde{\chi}_2^0$). In SUSY models with a bino-like $\widetilde{\chi}_1^0$, and wino-like $\widetilde{\chi}_1^+$ and $\widetilde{\chi}_2^0$, the two latter states would be almost degenerate, justifying the use of a common mass ($m(\widetilde{\chi})$). We consider decay chains proceeding via intermediate sleptons or sneutrinos, resulting in di- or multilepton final states. For small mass splittings the leptons in the final state would be soft and therefore compatible with the signal scenario of the

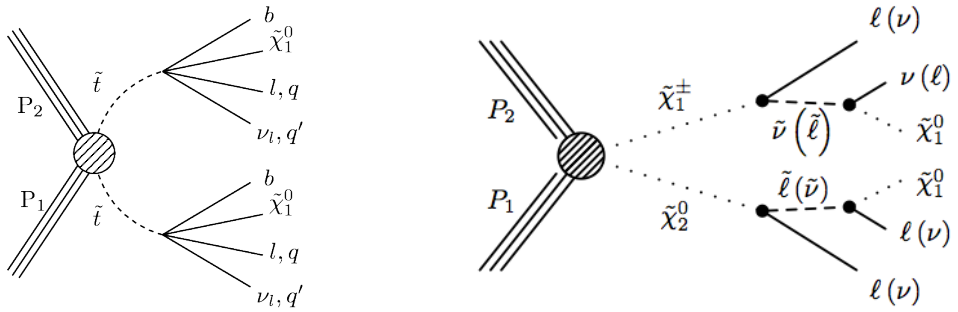

Figure 1: Signal models for (left) top squark pair production with subsequent four-body decays, and (right) chargino-neutralino pair production with decays via sleptons and sneutrinos.

dilepton search. Previous LHC results for these scenarios and mass splittings below $m(Z)$ can be found in Refs. [20–22]. The two signal models used in this document are shown in Fig. 1.

This document is organized as follows. The CMS detector, and the reconstruction and identification of objects are described in Section 2. Data and simulated samples used in this analysis are the subject of Section 3. Section 4 (5) is devoted to the search in the single-lepton (dilepton) channel. Results are summarized in Section 6 and conclusions are drawn in Section 7.

2 Detector and object definition

The CMS detector has been described in detail in Ref. [23]. Its central feature is a superconducting solenoid providing a homogeneous field of 3.8 T in a volume containing a silicon pixel and strip tracker, a lead tungstate crystal electromagnetic calorimeter, and a brass-scintillator hadron calorimeter. Muons are measured in gas-ionization chambers embedded in the steel flux-return yoke surrounding the solenoid. The acceptance of the silicon tracker and the muon systems extends to pseudorapidities of $|\eta| < 2.5$ and < 2.4, respectively. The barrel and endcap calorimeters cover the range $|\eta| < 3.0$ and are complemented by extensive forward calorimetry. The measurement of jets and $E_{\mathrm{T}}^{\mathrm{miss}}$ is based on particle candidates reconstructed by the particle-flow algorithm [24], which identifies leptons, photons, and charged and neutral hadrons combining information from all subdetectors. Particle candidates are clustered into jets using the anti-k_{T} algorithm with a distance parameter of 0.5. Jets are required to have $p_{\mathrm{T}} > 30\,\mathrm{GeV}$ and $|\eta| < 4.5$, and to pass loose quality criteria based on the energy fractions associated with electromagnetically or hadronically interacting charged or neutral particles. The negative vector sum of the transverse momenta of the PF candidates defines the value of $E_{\mathrm{T}}^{\mathrm{miss}}$ and the corresponding direction. Jet energies and $E_{\mathrm{T}}^{\mathrm{miss}}$ are corrected for shifts in the energy scale, contributions from additional, simultaneous proton-proton collisions (pileup), and residual differences between data and simulation. Jets originating from b-quarks are identified ("tagged") using the combined secondary vertex algorithm [25, 26] at a working point corresponding to an efficiency of about 70%.

Muons and electrons are required to have p_{T} above 5 and 7 GeV, respectively. In the single-muon search the lepton acceptance is restricted to $|\eta| < 2.1$ while in the dilepton search this limit is tightened to 1.5 for both electrons and muons. Standard loose identification requirements [27, 28] are applied to reduce the background from non-prompt leptons produced in semileptonic hadron decays, and from jets showing a lepton signature. Further background reduction is achieved by requiring the leptons to be isolated. The absolute isolation I_{abs} is computed by summing the transverse momenta of particle candidates in a cone of size $\Delta R < 0.3$, with $\Delta R \equiv \sqrt{\Delta\phi^2 + \Delta\eta^2}$ and ϕ the azimuthal angle. The energy in the isolation cone is corrected for the effects of pileup. The relative isolation I_{rel} is obtained by normalizing this value

to the p_T of the lepton. The details of the isolation requirements differ between the single- and dilepton topology due to differences in the dominant backgrounds and the purities. They are described in Sections 4 and 5.

3 Samples and event preselection

The data sample comprises proton-proton collisions recorded in 2012 at a centre-of-mass energy of 8 TeV and corresponding to an integrated luminosity of $19.7\,\text{fb}^{-1}$. The search uses events passing one of several online E_T^{miss} selections. These triggers evolved over the data taking period and require either $E_T^{miss} > 120\,\text{GeV}$, where E_T^{miss} is reconstructed from the energy deposited in the calorimeters, or $E_T^{miss} > 95\,\text{GeV}$ and a central jet with $p_T > 80\,\text{GeV}$, where both quantities are reconstructed using the PF algorithm. In the second part of the data taking period the threshold on E_T^{miss} was raised from 95 to 105 GeV. Control samples were collected based on a single-muon trigger with a p_T threshold of 24 GeV.

Simulated Monte Carlo (MC) samples of standard model background events are produced using a variety of generators. Single and pair production of top quarks are simulated using the POWHEG program. Simulations of multijet and diboson events are done with PYTHIA 6 [29]. The generation of all other relevant samples, in particular Z/γ^* processes, W+jets events, and $t\bar{t}$ production in association with a W, Z or Higgs boson is performed with the MADGRAPH [30] generator. Alternative samples of $t\bar{t}$ and diboson events are also produced using MADGRAPH. All samples generated with MADGRAPH are passed to PYTHIA 6 for hadronization and showering. The detector response is simulated by the GEANT4 [31] program. Finally, all events are reconstructed with the same algorithms as the ones used for data. Pileup events are included in the simulation and all samples are reweighted in order match the luminosity profile in data. Uncertainties related to this reweighting procedure are evaluated by varying the minimum bias cross section by 5%.

The signal simulation for $\tilde{t}$ pair production is done on a grid in the $\tilde{t} - \tilde{\chi}_1^0$ mass plane with $m(\tilde{t})$ ranging from 100–400 GeV, and $\Delta m \equiv m(\tilde{t}) - m(\tilde{\chi}_1^0)$ ranging from 10–80 GeV. The production of top squark pairs with up to two additional jets, and the four-body decays of the top squarks are generated by MADGRAPH. Chargino-neutralino pair production is also modelled with MADGRAPH, while the decays are generated by PYTHIA. A range in the common gaugino mass of 100–400 GeV is covered at a mass difference of 20 GeV to the $\tilde{\chi}_1^0$. As for the background samples, the generation steps for both signal models are followed by hadronization and showering in PYTHIA. For the signal samples the modelling of the detector response is performed with the CMS fast simulation program [32].

The effects of residual differences between data and simulation are taken into account in the analysis. The systematic uncertainty related to possible variations in the jet energy scale is evaluated by a coherent change of all jet energies, which is also propagated to E_T^{miss}. The jet energy resolution in simulation is found to be slightly better than in data. In order to compensate for this effect the energies of simulated jets are smeared, and a corresponding systematic uncertainty is assigned. Differences between data and simulation in the efficiencies of the reconstruction of leptons, and of the identification of leptons and b-jets, are compensated by scale factors. The uncertainties on these scale factors are propagated to the final results.

A first step in the event selection is designed to match the online requirements and to serve as a common basis for the analysis in both channels. It is guided by the general characteristics of signal events. The leading jet of each event is considered as an ISR jet candidate. It is required to pass tighter jet identification criteria and to fulfil $p_T > 110\,\text{GeV}$ and $|\eta| < 2.4$. Since jets

and leptons resulting from $\tilde{t}$ decays tend to be soft, at most one more jet with $p_T > 60\,\text{GeV}$ is accepted. At least one identified muon with $p_T > 5\,\text{GeV}$ and $|\eta| < 2.1$ must be present. Finally, a requirement of $E_T^{miss} > 200\,\text{GeV}$ is imposed. Using a control sample collected with the single-muon trigger the signal triggers are found to be fully efficient after these preselection criteria are applied.

4 Search in the single-lepton channel

The single-lepton topology is selected by requiring a single muon within the acceptance described in the previous sections. In order to avoid strong variations of the muon identification efficiency with p_T a combined isolation criterion, $I_{abs} < 5\,\text{GeV}$ or $I_{rel} < 0.2$, is used, equivalent to a transition from an absolute to a relative isolation requirement at $p_T = 25\,\text{GeV}$. Events are rejected if an electron, a τ lepton, or an additional muon with $p_T > 20\,\text{GeV}$ is present. Throughout this analysis the correlation between E_T^{miss} and the scalar sum of the transverse momenta of all jets, H_T, is taken into account by applying selections on the combined variable $C_T \equiv \min(E_T^{miss}, H_T - 100\,\text{GeV})$. In order to match the preselection $C_T > 200\,\text{GeV}$ is required. Background from SM di- and multijet production is suppressed by requiring the azimuthal angle between the momentum vectors of the two leading jets to be smaller than 2.5 rad for all events with a second hard jet of $p_T > 60\,\text{GeV}$. According to simulation the remaining sample is dominated by W+jets and, to a lesser extent, by $t\bar{t}$ production with a single, prompt lepton in the final state. Therefore we use the transverse mass computed from the muon momentum and the E_T^{miss} vector, m_T, as a discriminating variable.

Distributions of the muon p_T and of m_T at this stage of the selection are presented in Fig. 2. They show good agreement between data and simulation, the main characteristics of the signal, and the difference between signal distributions at two mass splittings.

In order to maintain sensitivity over a large range of Δm values several signal regions are defined. Since signal leptons have low momenta we impose an upper limit of $p_T < 30\,\text{GeV}$ in all these selections. As the muon p_T spectra of the signal change rapidly with Δm, the full range is subdivided into three bins in the calculation of the final results: 5–12 GeV, 12–20 GeV, and 20–30 GeV.

The region SRSL1 is designed for low values of Δm, where the b-jets produced in the $\tilde{t}$ decays rarely pass the selection thresholds. A veto on b-tagged jets strongly reduces the contribution from $t\bar{t}$ events. In addition, only events with negatively charged muons are accepted, using the fact that the remaining W+jets background shows significantly more positively charged muons while the signal is symmetric in the muon charge. In SRSL1 the acceptance for muons is reduced to the central region, $|\eta| < 1.5$, and the requirement on C_T is tightened to 300 GeV. For signal points at low Δm, m_T is typically small, mainly due to the soft lepton momentum spectrum. With increasing Δm the average m_T increases and eventually the distribution extends to values above $m(W)$. In order to cover the full range of Δm values SRSL1 is therefore divided into three subregions, SRSL1a–c, defined by $m_T < 60\,\text{GeV}$, $60 < m_T < 88\,\text{GeV}$, and $m_T > 88\,\text{GeV}$.

The second signal region SRSL2 targets signals with higher mass splitting, where some of the b jets enter the acceptance. Therefore, the b-jet veto in the low-momentum region ($30 < p_T < 60\,\text{GeV}$) is reverted and at least one such jet is required. Events with one or more b-tagged jets with $p_T > 60\,\text{GeV}$ are still rejected in order to reduce the $t\bar{t}$ background. In addition, the p_T threshold of the ISR jet candidate is raised to 325 GeV. This second signal region receives a strong contribution from $t\bar{t}$ events.

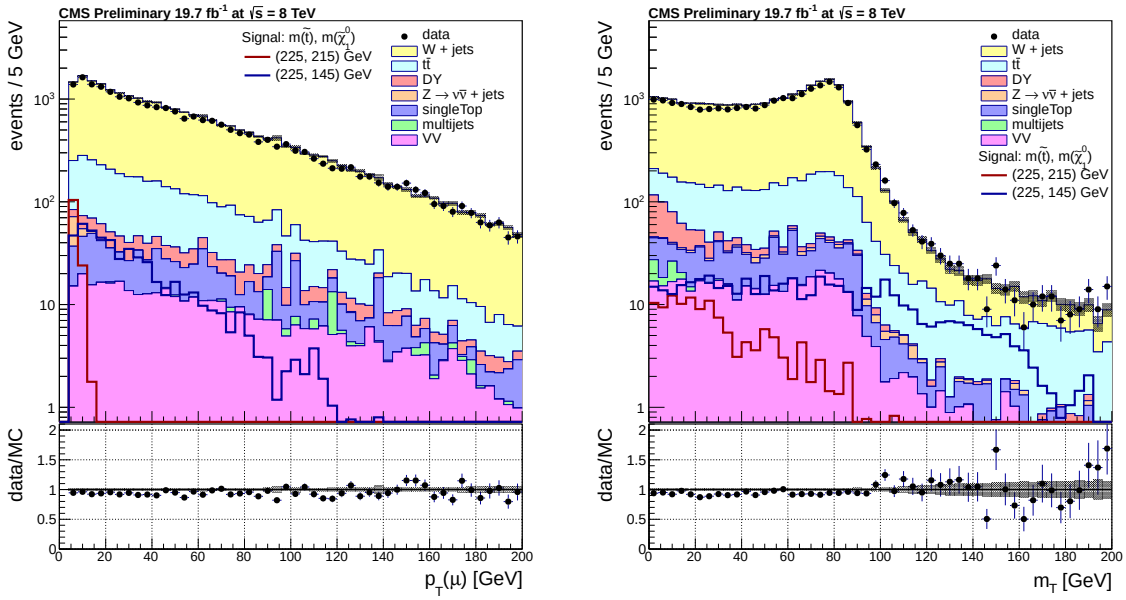

Figure 2: Distributions of (left) muon p_{T}, and (right) m_{T} after the preselection of the single-muon analysis. For each diagram the variable shown has been excluded from the selection. Data are indicated by circles. The uncorrected background predictions from simulation are represented as filled, stacked histograms, and the shapes for two signal points with $m(\tilde{\mathrm{t}}) = 225\,\mathrm{GeV}$ and mass splittings of $\Delta m = 10\,\mathrm{GeV}$ (80 GeV) as solid red (blue) lines. The error bars and the dark, shaded bands indicate the statistical uncertainties of data and simulation, respectively. The lower panels show the ratio of data to the sum of the SM backgrounds.

4.1 Background estimation

The following four background contributions are estimated using data: W+jets and $\mathrm{t\bar{t}}$ production, which are the dominant components for the single-muon search, $(\mathrm{Z} \to \nu\nu)$+jets, which is relevant for a signal region at high m_{T} as explained below, and multijet production. For the first three of these backgrounds data/simulation scale factors are determined in suitable control regions and applied to the simulated yields in the signal region. The contribution of multijet events is estimated using data only. Rare backgrounds (other Z/γ^* processes, diboson and single-top-quark production) are predicted using simulation.

Simulation provides only an imperfect description of the p_{T} spectrum for the main background samples (W+jets, $\mathrm{t\bar{t}}$). Since the extrapolations from control to signal regions involve the lepton p_{T} spectrum, the p_{T} distributions of both samples are corrected based on measurements in $\mathrm{t\bar{t}}$-, Z+jets-, and W+jets-dominated samples before deriving the scale factors.

For the estimation of the $\mathrm{t\bar{t}}$ background a single control region (CRSL($\mathrm{t\bar{t}}$)) is used: events are required to pass the basic selection defined above and must include at least two b-tagged jets, with one of them in the p_{T} region above 60 GeV. This control region has an estimated purity of 80% in $\mathrm{t\bar{t}}$ events. The observed event count in CRSL($\mathrm{t\bar{t}}$) is corrected for other background contributions and compared to the yield estimated from $\mathrm{t\bar{t}}$ simulation. The resulting scale factor of 1.05 is then used to modify the predictions of the $\mathrm{t\bar{t}}$ simulation in the different signal regions.

The W+jets yields from simulation are normalized in control regions associated to each of the four signal (sub-)regions SRSL1a–c (CRSL1a–c) and SRSL2 (CRSL2). Control and signal regions differ only by the muon p_{T} range: in the control regions a muon with $p_{\mathrm{T}} > 30\,\mathrm{GeV}$ is required. The control regions CRSL1a–c have an estimated purity of 80% in W+jets events. For

Table 1: Contributions to the control regions of the single-muon analysis as expected from simulation, together with the observed event counts. All uncertainties are statistical.

Background	CRSL($\mathrm{t\bar{t}}$)	CRSL1a	CRSL1b	CRSL1c	CRSL2
W+jets	67.9 ± 3.6	323.3 ± 6.4	141.9 ± 4.3	30.3 ± 2.0	36.5 ± 2.3
$\mathrm{t\bar{t}}$	471.0 ± 9.6	19.5 ± 2.2	9.9 ± 1.5	6.1 ± 1.2	37.5 ± 3.5
Z/γ^*+jets	2.1 ± 0.5	16.1 ± 1.0	0.8 ± 0.2	0.3 ± 0.1	0.7 ± 0.2
VV	3.8 ± 0.6	13.7 ± 1.3	8.0 ± 1.1	2.5 ± 0.5	1.1 ± 0.4
Single top	58.6 ± 12.6	4.6 ± 1.4	3.3 ± 1.2	1.1 ± 0.7	3.5 ± 1.2
Total SM	603.4 ± 16.2	377.1 ± 7.1	165.0 ± 4.8	40.3 ± 2.5	79.4 ± 4.3
Data	628	347	172	46	75

region CRSL2 this number is about 50%, the remainder being dominated by $\mathrm{t\bar{t}}$ events. Again, scale factors are derived after subtracting non-W+jets backgrounds from the observed yields in the control region. The $\mathrm{t\bar{t}}$ yields used in the subtraction are corrected by the scale factor determined as described in the previous paragraph. The scale factors for W+jets simulation vary from 0.83–1.18 in the four signal regions SRSL1a–c and SRSL2. Each factor is applied to all three muon p_T bins of a signal region; systematic uncertainties related to the shape of the p_T spectrum are assigned as described later in this section. The expected composition of the events in the control regions is summarized in Table 1.

After applying the signal selection with the exception of the requirement on muon p_T, the muon p_T spectra of $\mathrm{t\bar{t}}$ and W+jets events are similar. Therefore the correction procedure leads to an anti-correlation of the estimates for the two categories, and a relative uncertainty in the sum of the two contributions, which is smaller than the uncertainty of a single component. For this reason an alternative background estimation procedure, which applies the normalization at high muon p_T described above to the sum of both backgrounds, yields almost identical results in terms of the total background.

The extrapolation of the correction factors from control to signal regions has been validated by comparing corrected yields from simulation to data in sideband regions. Each of these sidebands is defined by one of the following changes with respect to the signal selection: (a) a lowering of the $E_\mathrm{T}^\mathrm{miss}/H_\mathrm{T}$ requirement to $200 < C_\mathrm{T} < 300\,\mathrm{GeV}$, (b) a change in the muon charge requirement, and (c) the condition of exactly one b-tagged jet with $p_\mathrm{T} > 60\,\mathrm{GeV}$. The predictions in the sidebands are compatible with the observations, and the results are used to assign systematic uncertainties on the extrapolation of the scale factors to the signal regions. These uncertainties are 20% for the estimate of the $\mathrm{t\bar{t}}$ background, and 10–30% for the estimate of the W+jets background.

At high values of m_T only few W+jets events pass the SRSL1c selection. In this signal region Z+jets production, with the Z boson decaying to neutrinos and a non-prompt muon related to one of the jets, constitutes a non-negligible contribution. Again, the size of this contribution is estimated from simulation, together with a correction derived from data. As a control sample, Z+jets events with Z boson decays to muon pairs are used, selected by the single-muon trigger. Using tighter muon selection criteria and a selection on the mass of the dimuon system a high purity sample is obtained. The events are used to mimick $\mathrm{Z} \to \nu\nu$ decays by removing the two leading muons and adding their momenta to the $E_\mathrm{T}^\mathrm{miss}$ vector. The correction is applied as the product of two factors: $R_{\mu\mu}$, the inclusive data-to-simulation ratio, and the ratio of the probabilities to observe a third, soft muon ($R_{\mu\mu\mu/\mu\mu}$). The first factor corrects the cross section in the $\mu\mu$ channel for a signal-like region. Its measured value is 0.80 ± 0.03. The double ratio $R_{\mu\mu\mu/\mu\mu}$ is determined in a looser selection to be 1.26 ± 0.27, yielding a total correction factor

Table 2: Estimated background contributions to the signal regions of the single-muon analysis. The expected yields for two signal points are also shown (the numbers in parentheses indicate $m(\tilde{t})$ and $m(\tilde{\chi}_1^0)$). All uncertainties are statistical.

Background	SRSL1a	SRSL1b	SRSL1c	SRSL2
W+jets	116.8 ± 8.8	73.2 ± 7.6	8.8 ± 2.1	16.0 ± 4.9
$t\bar{t}$	7.4 ± 1.3	4.1 ± 1.0	1.2 ± 0.5	13.8 ± 1.8
$Z \to \nu\nu$+ jets	1.1 ± 0.4	1.2 ± 0.4	1.5 ± 0.5	0.3 ± 0.2
Z/γ^*+jets (other)	4.4 ± 0.5	0.2 ± 0.1	0.2 ± 0.1	0.5 ± 0.2
VV	4.6 ± 0.7	1.8 ± 0.5	0.7 ± 0.3	0.5 ± 0.2
Single top	0.1 ± 0.1	0.6 ± 0.4	< 0.3	1.0 ± 0.7
Total SM prediction	134.5 ± 8.9	81.3 ± 7.8	12.3 ± 2.3	32.1 ± 5.3
$\tilde{t}\bar{t}$ signal (250,230)	32.5 ± 2.8	6.2 ± 1.2	4.7 ± 1.0	7.1 ± 1.3
$\tilde{t}\bar{\tilde{t}}$ signal (300,250)	11.0 ± 1.0	4.2 ± 0.6	5.1 ± 0.7	10.7 ± 1.0

of 1.01 ± 0.22. Systematic uncertainties due to the evolution with $E_{\mathrm{T}}^{\mathrm{miss}}$ and H_{T}, or due to differences in the muon efficiency or acceptance between data and simulation, are negligible with respect to the statistical uncertainty.

The contribution from multijet events is estimated by inverting the requirements on muon isolation, muon impact parameter, and the veto on leading jets in back-to-back configuration. Assuming small correlations between the three variables mentioned above, the amount of multijet events can be estimated using the yield from in the fully inverted selection and the product of three reduction factors (one for each variable). The estimated contributions to SRSL1 and SRSL2 are below 0.1 events and are therefore neglected. A summary of the expected contributions of different background processes to the signal regions is shown in Table 2 together with the yields of two benchmark signal points.

4.2 Systematic uncertainties

In addition to systematic uncertainties estimated in the previous subsections the following systematic effects and associated uncertainties have been evaluated.

The full difference in the background estimates induced by the correction of the p_{T} spectrum of simulated $t\bar{t}$ and W+jets events is assigned as a systematic uncertainty.

Changes in the polarization of the W boson can have an impact on the results since they change the balance between muon p_{T} and $E_{\mathrm{T}}^{\mathrm{miss}}$. In order to quantify this effect the polarization fractions $f_{\lambda=+1}$, $f_{\lambda=-1}$, and $f_{\lambda=0}$, associated with helicity +1, helicity +1, and helicity 0 amplitudes have been modified following three different scenarios: a 10% variation to $f_{-1} - f_{+1}$ for both W^+ and W^-, a 5% variation of f_{-1}, f_{+1}, and a 10% variation to the longitudinal polarization fraction, f_0 [33–35].

The uncertainties based on the comparison of data and simulation in the validation regions described in the previous subsection are propagated to the final estimate. An uncertainty of 50% is assigned to the cross sections of all non-leading backgrounds, including $Z \to \nu\nu$, and propagated through the full estimation procedure. An overview of all systematic uncertainties related to the background prediction is presented in Table 3. The dominant uncertainties are related to the limited statistical precision of the validation procedure and to the uncertainties on the shape of the muon p_{T} spectrum in W+jets events.

Table 3: Relative systematic uncertainties (in %) on the background predictions in the signal regions of the single-muon search.

Systematic effect	SRSL1a	SRSL1b	SRSL1c	SRSL2
Pileup	0.5	0.8	3.0	0.5
Wp_{T} reweighting	7.1	8.8	8.1	3.7
$\mathrm{t\bar{t}}$ p_{T} reweighting	0.8	0.5	0.1	5.4
Jet energy scale	2.4	3.2	2.1	6.0
Jet energy resolution	1.1	4.4	7.3	3.4
b tagging	0.1	0.1	0.5	1.3
Wpolarization	2.9	2.8	3.9	0.8
Muon efficiency	3.5	3.5	3.5	3.5
W+jets validation	8.8	18.1	21.7	10.2
$\mathrm{t\bar{t}}$ validation	1.0	0.9	1.7	8.4
Non-leading backgrounds	3.8	2.4	9.8	3.6
Total uncertainty	13.1	21.5	27.0	17.1

5 Search in the dilepton channel

The analysis in the dilepton channel also starts from the common baseline selection described in Section 3. In this topology less background is expected and thus the selection on $E_{\mathrm{T}}^{\mathrm{miss}}$ and the p_{T} of the ISR jet candidate are set to be above 200 GeV and 150 GeV, respectively, just above the trigger thresholds. As the relative fraction of reconstructed leptons not stemming from a Z or W boson ("non-prompt" leptons) is higher the isolation and identification criteria on the leptons are stricter. On top of the muon identification used for the single-lepton topology, stricter requirements on the number of tracker hits, the quality of the track fit, and the match to signals in the muon stations are applied. This selection is similar to the soft muon identification used for b-quark physics in CMS. For electrons the definitions for the H→ZZ→4l [36] analysis are used together with a stronger rejection of photon conversions. For both lepton flavors $I_{\mathrm{abs}} < 5\,\mathrm{GeV}$ and $I_{\mathrm{rel}} < 0.5$ is required and impact parameter values with respect to the vertex in transverse and longitudinal plane of 0.01 cm. As in the region SRSL1 of the single-lepton analysis b-tagged jets are vetoed to suppress $\mathrm{t\bar{t}}$ backgrounds. To remove potential multijet backgrounds a selection on $E_{\mathrm{T}}^{\mathrm{miss}}/H_{\mathrm{T}} > 2/3$ is applied.

After this selection one of the main backgrounds is Z/γ^* production of τ pairs, with both τ leptons decaying leptonically. Under the assumption that the direction of the reconstructed lepton is parallel to the τ direction, which is true to good approximation, the invariant mass of the τ pair ($m_{\tau\tau}$) can be reconstructed by setting its transverse momentum equal to the measured hadronic recoil. All events with $m_{\tau\tau} < 160\,\mathrm{GeV}$ are rejected. In order to increase sensitivity we select events in two regions defined by the p_{T} of the leading lepton: 5–15 GeV, and 15–25 GeV. The second lepton is required to have $p_{\mathrm{T}} < 15\,\mathrm{GeV}$. We require exactly two identified leptons of opposite sign, with at least one of them a muon. Finally events with an invariant mass of the dilepton pair $< 5\,\mathrm{GeV}$ are rejected in order to remove a region that is difficult to simulate and to avoid any potential J/ψ background.

5.1 Background Prediction

Four different backgrounds categories are predicted using data: dileptonic $\mathrm{t\bar{t}}$ events ($\mathrm{t\bar{t}}(2\ell)$), which constitute the largest background (Table 5); diboson production such as WW or WZ (the second-largest background); Z/γ^* production of τ pairs with leptonic τ decays. Backgrounds with one non-prompt (NP) lepton, i.e. W+jets and semileptonic $\mathrm{t\bar{t}}$ events ($\mathrm{t\bar{t}}(1\ell)$), are the forth

category. Half of the background events contain at least one leptonically decaying τ lepton. The negligible ($\approx$ 1%) contribution of rare processes ($t\bar{t}$ W,$t\bar{t}$ Z,$t\bar{t}$ H,tW, W^-W^-, W^+W^+) is predicted using simulation. For each of the four categories a control region (CR), enriched in such processes, is defined in data, from which we derive correction factors to correct yields from simulation.

In all control regions the requirements on jets are the same as in the signal region. Several control regions use events with higher lepton p_T compared to the signal region. In these regions the leading lepton has to be a muon, and events are selected using the single-muon trigger described before. The relative lepton isolation has to be smaller than 0.12, and the muon identification criteria are tightened. Apart from the Z/γ^* control region the E_T^{miss} requirement is lowered to 125 GeV, and the E_T^{miss} selection of the signal region is instead applied to L_T, the sum of E_T^{miss} and the p_T of the leading lepton. The actual L_T cut is > 225 GeV to take into account that for the default selection L_T is also up to 25 GeV higher than E_T^{miss}. In this way the event yields in the CRs can be increased while maintaining kinematics similar to the signal region even in the presence of a higher p_T lepton.

In order to achieve a clean control sample of dileptonic $t\bar{t}$ events (CRDL($t\bar{t}(2\ell)$)) we require exactly one b-tagged jet. This jet must not be the leading jet, since such a veto ensures a similar distribution of the p_T of the $t\bar{t}$ system as in the signal region. We require one muon with $p_T > 25$ GeV and a sub-leading lepton with $p_T > 15$ GeV. Backgrounds other than $t\bar{t}(2\ell)$ are subtracted from data before calculating the ratio between data and the prediction from simulation for $t\bar{t}(2\ell)$ in the control region. This ratio is used to rescale the simulated $t\bar{t}(2\ell)$ yields in the signal region.

As control region for non-prompt leptons (CRDL(NP)) we use events with leptons of the same charge. It was checked that in the selected kinematic region the origins for NP leptons, mainly heavy quarks, occur at a similar fraction as in the signal region. Also the kinematics of these non-prompt leptons is very similar in signal and control region. In order to increase the number of events in CRDL(NP) also same-sign events with a leading lepton p_T above 25 GeV are used. Also under these conditions origins and kinematics of the non-prompt leptons are similar between signal and control regions, since the NP contribution in the signal region is mostly related to the sub-leading lepton. Again the data yield in the control region is corrected for other backgrounds such as diboson events. The ratio of the corrected yield to the simulated NP yield in the CR is used to rescale the simulated NP yield in the signal region.

For the prediction of Z/γ^* events two separate control regions are defined. The first one is used to correct for any effects on $m_{\tau\tau}$. For this purpose a clean sample of Z/γ^* events with decays to a pair of muons is used. The invariant mass of the muon pair has to be higher than 10 GeV, and the E_T^{miss} selection is applied to the transverse momentum of the muon pair. Three bins are defined as a function of this momentum: 200–300 GeV, 300–400 GeV, and >400 GeV. We use the reconstructed muon pair p_T to measure the resolution of the hadronic recoil along and perpendicular to direction given by the muon pair both in data and simulation. The resulting scaling factors of the recoil resolution are applied to the simulation in order to recompute the efficiency of the $m_{\tau\tau}$ selection in the signal region. A second control region (CRDL(Z)) is used to measure in data the probability of Z/γ^* events leading to two soft leptons and very high E_T^{miss}. In order to do so the selection on $m_{\tau\tau}$ is inverted. After subtracting other backgrounds in this region, the observed yield is multiplied with the corrected $m_{\tau\tau}$ efficiency to predict the number of Z/γ^* events in the signal region.

For the diboson control region (CRDL(VV)) one muon with $p_T > 25$ GeV is required. The p_T of the second lepton has to be above 15 GeV. To further enhance the diboson fraction and

reduce the otherwise dominant $t\bar{t}$ background at most two jets are allowed, events with a jet passing a looser working point of the b-tagging algorithm are rejected, and the azimuthal angle between the leading lepton and the leading jet has to be > 1 rad. Finally we require M_{ll} to be above 50 GeV. Contributions of $t\bar{t}(2\ell)$, NP, and Z/γ^* to CRDL(VV) are estimated with methods similar to those used for the signal region. Backgrounds due to rare processes are subtracted using the simulation. After this correction the ratio of the number of data to simulated diboson events is built and used to rescale the simulated VV yield in the signal region.

The background contribution from multijet events is negligible in our final selection. Apart from the fact that we require high $E_{\mathrm{T}}^{\mathrm{miss}}$ and two leptons, we also apply a cut on the $E_{\mathrm{T}}^{\mathrm{miss}}/H_{\mathrm{T}} > 2/3$ to reject any residual multijet events. A test, to evaluate the efficacy of such a cut, was performed by inverting the cut to have a region that should have significant multijet background if there would be any. For this region, data yields were compared with the simulation results that do not include multijet events and were found in agreement. Further tests by including the electron-electron channel (usually not in our selection) and by relaxing the D_{xy} and D_z cuts to 0.05 cm showed again an agreement. These tests confirmed that, as expected, we can assume that multijet background is negligible in our final selection that employs much tighter cuts against multijet events.

The event yields for data and simulation in the different control regions are shown in Table 4. The predicted event yields per background for each search bin are presented in Table 5.

Table 4: Contributions to the control regions of the dilepton analysis as expected from simulation, together with the observed event counts. All uncertainties are statistical.

Background	CRDL($t\bar{t}(2\ell)$)	CRDL(NP)	CRDL(VV)	CRDL(Z)
$t\bar{t}(2\ell)$	119.1±2.4	0.27±0.11	30.3±1.2	0.15±0.08
$t\bar{t}(1\ell)$	1.09±0.29	4.7±0.6	0.30±0.14	0.11±0.11
W+jets	<0.4	3.4±1.3	<0.4	0.7±0.7
Z/γ^*+jets	0.4 ±0.4	<0.30	4.9±1.3	2.8±0.9
VV	2.4 ±0.6	0.62±0.11	45.9±1.8	0.13±0.09
Rare backgrounds	14.9±2.7	1.0±0.5	6.4±1.7	<0.21
Total SM	138.0±3.7	10.0±1.5	87.8±3.0	3.9±1.1
Data	119	11	81	5

Table 5: Predicted background yields for the two signal region bins of the dilepton search. The sample names are explained in the text. For the signal samples $m(\widetilde{t})$ and $m(\widetilde{\chi}_1^0)$ are shown in parentheses.

Background	$p_{\mathrm{T}}(\ell_1)$: 5–15 GeV	$p_{\mathrm{T}}(\ell_1)$: 15–25 GeV	Inclusive
$t\bar{t}(2\ell)$	0.75 ±0.19	2.08 ±0.37	2.84 ±0.42
$t\bar{t}(1\ell)$,W+jets	0.60 ±0.33	1.32 ±0.69	1.92 ±0.76
Z/γ^*+jets	<0.30	0.48 ±0.45	0.48 ±0.45
VV	0.74 ±0.27	1.61 ±0.48	2.35 ±0.55
Rare backgrounds	0.03 ±0.01	0.08 ±0.04	0.11 ±0.04
Total SM	2.12 ±0.47	5.6 ±1.0	7.7 ±1.1
$\widetilde{t}\widetilde{t}$ signal (250,230)	10.0 ±1.5	3.41 ±0.90	13.5 ±1.8
$\widetilde{t}\widetilde{t}$ signal (300,250)	3.98 ±0.61	3.83 ±0.58	7.80 ±0.84

In order to test the prediction methods we defined several validation regions, which are enriched in specific backgrounds, but expected to be free of signal. A first region is equivalent to

the signal region, except for an inversion of the veto on b-tagged jets. This region is used to test the prediction of low p_{T} leptons in $\mathrm{t\bar{t}}(2\ell)$ events. A further validation region is identical to CRDL($\mathrm{t\bar{t}}(2\ell)$), except that the p_{T} of the sub-leading lepton is required to be below 15 GeV. This region provides a further test of the prediction of the soft lepton rate. A further validation region is the same as CRDL(VV), apart from the fact that all selections used to enrich the region in diboson events are inverted. Also a validation region which has a composition in backgrounds similar to the signal region is defined. For this one muon with p_{T} above 25 GeV is required, while the second lepton must be soft ($p_{\mathrm{T}} < 15$ GeV). All regions show reasonable agreement.

5.2 Systematic uncertainties

In addition to the common uncertainties from object reconstruction and simulation, described in Sections 2 and 3, the following systematic uncertainties that are specific to the individual background predictions are considered.

In the estimate of the $\mathrm{t\bar{t}}(2\ell)$ background the polarization of the W boson resulting from the t quark decay is varied. In addition, the spin correlation between the two t quarks is changed by 10%, as this might affect how often both leptons are soft [37]. As in the single-lepton channel, the full difference due to the reweighting of the top p_{T} spectrum in $\mathrm{t\bar{t}}$ simulation is taken as a further uncertainty. However, its effect is small due to the background prediction method used.

In order to assess the uncertainty related to the estimate of NP backgrounds the fractions of leptons from b- and c-hadrons are varied by 50% and 100%, respectively. The relative fraction of $\mathrm{t\bar{t}}$ to W+jets events is altered by rescaling both contributions by $\pm 50\%$. The largest of these variations is used as uncertainty. Furthermore, the p_{T} and $|\eta|$ distributions in the control region are varied to reflect potential residual differences in the kinematics between signal and control region. Also the polarization of the W boson is varied to estimate the uncertainty due to polarization modelling.

The cross sections for WW [38, 39] and also WZ and ZZ production have been measured at the LHC, and even differential distributions show reasonable agreement. To estimate the uncertainties related to VV production the polarization of the vector bosons is altered by 10%, as well as the fraction of the diboson pair momentum that a single boson carries. In addition, the cross section corresponding to events with $m(\gamma^*)$ between 1 and 12 GeV is varied by 100%, in order to account for any potential shape mismodelling of the dilepton mass (the lowest $m(\gamma^*)$ region is already excluded by the minimum dilepton mass requirement of 5 GeV applied in this analysis).

In the estimation of the Z/γ^* background the effect of the resolution correction is used to derive an uncertainty due to a potential mismodelling of the resolution. The cross section of rare processes is varied by $\pm 50\%$ throughout the analysis (also in the control regions), and the effect is propagated to the event yields in the signal region.

A summary of all uncertainties can be found in Table 6. The by far dominating uncertainty stems from the limited number of simulated events.

6 Results and interpretation

The observations and background predictions for the signal regions of the single- and dilepton searches are summarized in Table 7. Observed and predicted yields are in good agreement and give no indication of the presence of signal. The modified-frequentist $\mathrm{CL_S}$ method [40–42]

with a one-sided profile likelihood ratio test statistic is used to define 95% confidence level (CL) upper limits on the production cross section as a function of the $\widetilde{t}$ and $\widetilde{\chi}_1^0$ masses. Statistical uncertainties related to the observed number of events in control regions are modelled as Poisson distributions. All other uncertainties are assumed to be multiplicative and are modelled with lognormal distributions. The impact of a potential signal contamination in the control regions is taken into account in the calculation of the limits for each signal point.

Systematic uncertainties on signal yields related to the determination of the integrated luminosity [43], pileup, energy scales, object identification efficiencies, and uncertainties in the parton distribution functions [44–48] and the modelling of ISR [49] have been evaluated. The dominant term is related to ISR and amounts to approximately 20%. Correlations between the systematic uncertainties in different signal regions are taken into account, where applicable.

The limits obtained for top squark pair production in the single-muon and the dilepton search are shown in Fig. 3 left and right, respectively, under the assumption of a 100% branching ratio of the four-body decay. Using the $\widetilde{t}$ pair production cross section calculated at next-to-leading order (NLO) + next-to-leading logarithm (NLL) precision [50–55] the cross section limits can be converted into excluded regions in the $\widetilde{\chi}_1^0$–$\widetilde{t}$ mass plane. At $\Delta m \approx 25\,\text{GeV}$ the dilepton search excludes $\widetilde{t}$ masses below 316 GeV. The single-lepton search shows a smaller reach in $m(\widetilde{t})$ ($\approx$ 250 GeV) but has a higher sensitivity at the lowest considered mass splitting of 10 GeV, where values up to $\approx$ 210 GeV are excluded. Here and in the following all quoted values for mass limits refer to the -1σ variation of the predicted cross section. In the intermediate Δm region ($\approx$ 20–70 GeV) these results considerably extend existing limits [18, 19]. They are complementary to the results of searches in the monojet topology targeting the decay to $c\widetilde{\chi}_1^0$ [17, 18].

In the case of chargino-neutralino pair production the results of the dilepton analysis are used, and two models are studied. If only the partners of left-handed leptons ($\widetilde{\ell}_L$) and neutrinos ($\widetilde{\nu}$) participate in the process, we expect a "flavour-democratic" scenario with identical branching fractions into all lepton flavours, both for the chargino and the neutralino. In this scenario the fraction of events with at least two charged leptons is reduced by 50% due to the $\widetilde{\chi}_2^0 \to \nu\nu\widetilde{\chi}_1^0$ decay channel. If only the partners of right-handed leptons ($\widetilde{\ell}_R$) are involved the production of τ leptons is increased since the $\widetilde{\ell}_R$ would couple to the higgsino component of the chargino. For this case we use a τ-enriched scenario where the chargino decays exclusively to a τ lepton, while the neutralino decays democratically as in the first case. In our interpretation we

Table 6: Relative systematic uncertainties (in %) on the predicted yield in the signal regions of the search in the dilepton channel.

Systematic effect	$p_T(\ell_1)$: 5–15 GeV	$p_T(\ell_1)$: 15–25 GeV
Statistical uncertainty	21.9	18.3
Jet energy scale	1.0	2.8
b tagging	1.5	1.4
Electron efficiency	1.3	1.1
Muon efficiency	6.0	4.5
$\overline{\text{tt}}$ background	5.1	5.4
NP background	10.1	5.6
Z/γ^* background	0.0	2.3
VV background	8.0	2.6
Rare backgrounds	3.7	3.3
Total uncertainty	26.9	21.1

Table 7: Summary of observed, and expected background yields in the signal regions of the single- and dilepton searches. The uncertainties on the background yields include statistical and systematic contributions.

p_T (μ)		SRSL1a	SRSL1b	SRSL1c	SRSL2	p_T (ℓ_1)		SRDL
5–12	exp.	41.4 ± 6.3	29.7 ± 7.2	4.3 ± 1.5	11.3 ± 2.9	5–15	exp.	2.1 ± 0.6
GeV	obs.	42	17	3	16	GeV	obs.	2
12–20	exp.	44.2 ± 6.8	25.1 ± 6.2	3.1 ± 1.2	8.5 ± 2.4	15–25	exp.	5.6 ± 1.2
GeV	obs.	39	14	4	16	GeV	obs.	4
20–30	exp.	49.2 ± 7.5	26.5 ± 6.5	5.0 ± 1.8	12.2 ± 3.0			
GeV	obs.	40	28	5	9			
all	exp.	134.5 ± 19.8	81.3 ± 19.1	12.3 ± 4.0	32.1 ± 7.7	all	exp.	7.7 ± 1.4
	obs.	121	59	12	41		obs.	6

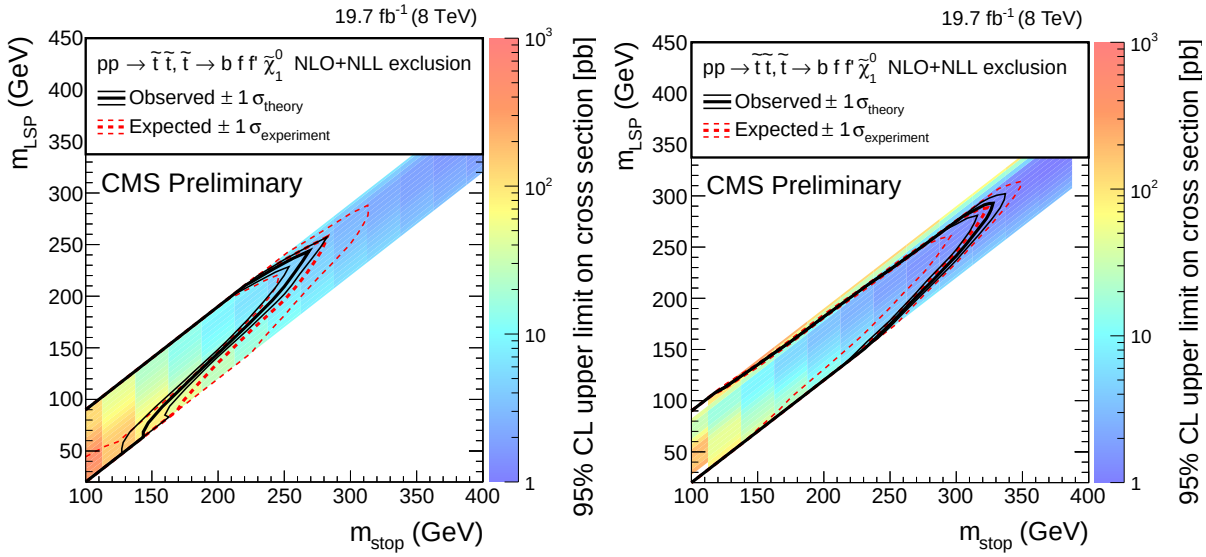

Figure 3: Cross section and mass limits at 95% CL in the $m(\tilde{\chi}_1^0)$ vs. $m(\tilde{t})$ mass plane for the (left) single-lepton and (right) dilepton search. The colour shading corresponds to the observed limit on the cross section. The solid (dashed) lines show the observed (expected) mass limits, with the thick lines representing the central value and the thin lines the variations due to the theoretical (experimental) uncertainties.

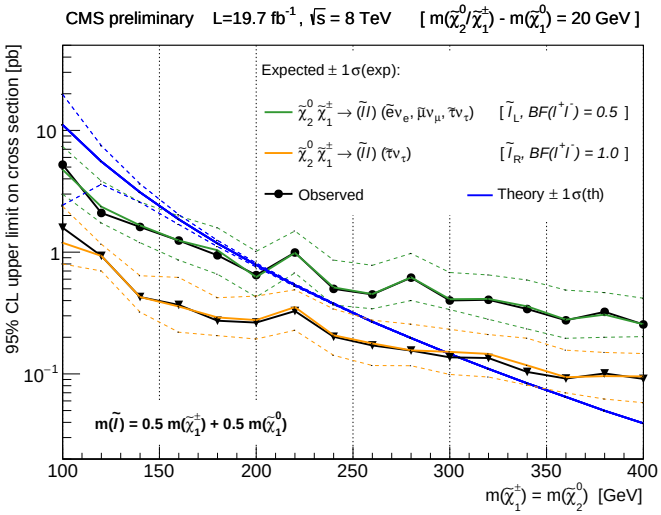

Figure 4: Cross section limits at 95% CL obtained from the search in the dilepton channel as a function of the common $\widetilde{\chi}_1^0/\widetilde{\chi}_1^+$ mass. The black lines with symbols correspond to the observed limit, while the solid and dashed coloured lines represent the expected limit and the $\pm 1\sigma$ bands corresponding to the experimental uncertainties, respectively. The flavour-democratic (τ-enriched) cases are indicated by green (orange) lines and circular (triangular) symbols. The solid and dashed blue lines correspond to the predicted cross section for chargino-neutralino production and its uncertainties.

assume $m(\widetilde{\ell}) = (m(\widetilde{\chi}_1^0) + m(\widetilde{\chi}_1^+))/2$. In Fig. 4 the 95% CL cross section limits are presented for the two cases in a compressed scenario with $m(\widetilde{\chi}_1^+) - m(\widetilde{\chi}_1^0) = 20\,\text{GeV}$, together with the predicted cross section for chargino-neutralino pair production. Comparing with the predicted cross section, calculated at NLO+NLL precision with the RESUMMINO [56–58] program, 95% CL limits on $m(\widetilde{\chi})$ of 204 GeV (304 GeV) are obtained for the flavour-democratic (τ-enriched) scenario. In this compressed scenario the new limits slightly improve current results in the flavour-democratic scenario and exceed them by $\approx 200\,\text{GeV}$ for the τ-enriched scenario [20], as for the latter the dominant decays lead to final states with opposite-sign leptons.

7 Conclusions

A search for supersymmetry with compressed mass spectra is performed in events with one or two hard jets, $E_{\text{T}}^{\text{miss}}$, and soft leptons, compatible with the emission of initial state radiation. In particular, the search targets the pair production of top squarks with a mass splitting of at most 80 GeV with respect to the LSP. The data sample consists of proton-proton collisions at $\sqrt{s} = 8\,\text{TeV}$, recorded by the CMS detector in 2012. Two topologies are considered: events with a single, soft muon, and events in which a second, soft electron or muon is present. Signal regions are defined requiring an ISR jet candidate, low jet multiplicity, and moderate to high values of $E_{\text{T}}^{\text{miss}}$. At low mass splitting lepton momenta are low, and the b-jets do not enter the acceptance. At higher values of Δm the average lepton momentum increases, and soft b-jets can be reconstructed. Therefore signal regions are further divided according to the p_{T} of the (leading) lepton and the presence or absence of a soft b-tagged jet. In the single-lepton search the transverse mass is used as an additional discriminating variable.

The main backgrounds to this search are W+jets and $\text{t}\bar{\text{t}}$ production. Contributions to the signal regions from these and several non-leading background sources are estimated using data in control regions to normalize the simulated yields. These estimates are validated with data in

alternative control regions.

The observations in the signal regions are compatible with the SM background predictions. In the absence of any indication for supersymmetry, cross section limits are set at 95% CL in the LSP - top squark mass plane. These limits are used to derive mass limits based on a reference cross section for top squark pair production and assuming a 100% branching ratio for the four-body decay $\widetilde{t} \to bff'\widetilde{\chi}_1^0$. The most stringent limit on the mass of the top squark is obtained in the dilepton channel: $m(\widetilde{t}) < 316\,\text{GeV}$ at 95% CL for a mass splitting of $\approx 25\,\text{GeV}$. These results extend existing limits in the four-body decay channel of the top squark [18, 19] and complement the analyses performed in the $\widetilde{t} \to c\widetilde{\chi}_1^0$ channel [17].

The results obtained in the dilepton channel are also used to set limits on models of chargino-neutralino production in a compressed spectrum with a mass difference between $\widetilde{\chi}_2^0/\widetilde{\chi}_1^+$ and $\widetilde{\chi}_1^0$ of 20 GeV. In the case of flavour-democratic leptonic decays of these particles 95% CL a lower limit on the common $\widetilde{\chi}_2^0/\widetilde{\chi}_1^+$ mass is set at 204 GeV. If chargino decays proceed exclusively via the τ channel this limit increases to 304 GeV.

References

[1] J. Wess and B. Zumino, "Supergauge transformations in four dimensions", *Nucl. Phys* **B70** (1974) 39, doi:10.1016/0550-3213(74)90355-1.

[2] H. P. Nilles, "Supersymmetry, Supergravity and Particle Physics", *Phys. Reports* **110** (1984) 1, doi:10.1016/0370-1573(84)90008-5.

[3] H. E. Haber and G. L. Kane, "The Search for Supersymmetry: Probing Physics Beyond the Standard Model", *Phys. Reports* **117** (1987) 75, doi:doi:10.1016/0370-1573(85)90051-1.

[4] R. Barbieri, S. Ferrara, and C. A. Savoy, "Gauge Models with Spontaneously Broken Local Supersymmetry", *Phys. Lett.* **B119** (1982) 343, doi:10.1016/0370-2693(82)90685-2.

[5] S. Dawson, E. Eichten, and C. Quigg, "Search for Supersymmetric Particles in Hadron - Hadron Collisions", *Phys. Rev.* **D31** (1985) 1581, doi:10.1103/PhysRevD.31.1581.

[6] E. Witten, "Dynamical Breaking of Supersymmetry", *Nucl. Phys.* **B188** (1981) 513, doi:10.1016/0550-3213(81)90006-7.

[7] S. Dimopoulos and H. Georgi, "Softly Broken Supersymmetry and SU(5)", *Nucl. Phys.* **B193** (1981) 150, doi:10.1016/0550-3213(81)90522-8.

[8] R. Barbieri and G. Giudice, "Upper Bounds on Supersymmetric Particle Masses", *Nucl. Phys.* **B306** (1988) 63.

[9] B. de Carlos and J. Casas, "One loop analysis of the electroweak breaking in supersymmetric models and the fine tuning problem", *Phys.Lett.* **B309** (1993) 320.

[10] S. Dimopoulos and H. Georgi, "Softly Broken Supersymmetry and SU(5)", *Nucl. Phys.* **B193** (1981) 150.

[11] E. Witten, "Dynamical Breaking of Supersymmetry", *Nucl. Phys.* **B188** (1981) 513.

[12] W. F. M. Dine and M. Srednicki, "Supersymmetric Technicolor", *Nucl. Phys.* **B189** (1981) 575.

[13] S. Dimopoulos and S. Raby, "Supercolor", *Nucl. Phys.* **B182** (1981) 353.

[14] S. Sakai, "Naturalness in Supersymmetric Guts", *Zeit. Phys.* **C11** (1981) 153.

[15] R. Kaul and P. Majumdar, "Cancellation of quadratically divergent mass corrections in globally supersymmetric spontaneously broken gauge theories", *Nucl. Phys.* **B199** (1982) 36.

[16] C. Balazs et al., "Dark matter, light stops and electroweak baryogenesis", *Phys. Rev. D* **70** (2004) 015007, doi:10.1103/PhysRevD.70.015007.

[17] CMS Collaboration, "Searches for third-generation squark production in fully hadronic final states in proton-proton collisions at $\sqrt{s} = 8$ TeV", CMS Physics Analysis Summary CMS-PAS-SUS-14-001, 2014. to be published.

[18] ATLAS Collaboration, "Search for top squark pair production in final states with one isolated lepton, jets, and missing transverse momentum in $\sqrt{s}$ =8 TeV pp collisions with the ATLAS detector", *JHEP* **1411** (2014) 118, doi:10.1007/JHEP11(2014)118, arXiv:1407.0583.

[19] ATLAS Collaboration, "Search for pair-produced third-generation squarks decaying via charm quarks or in compressed supersymmetric scenarios in pp collisions at $\sqrt{s} = 8$ TeV with the ATLAS detector", *Phys.Rev.* **D90** (2014), no. 5, 052008, doi:10.1103/PhysRevD.90.052008, arXiv:1407.0608.

[20] CMS Collaboration, "Searches for electroweak production of charginos, neutralinos, and sleptons decaying to leptons and W, Z, and Higgs bosons in pp collisions at 8 TeV", *Eur.Phys.J.* **C74** (2014), no. 9, 3036, doi:10.1140/epjc/s10052-014-3036-7, arXiv:1405.7570.

[21] ATLAS Collaboration, "Search for direct production of charginos and neutralinos in events with three leptons and missing transverse momentum in $\sqrt{s} = 8$TeV pp collisions with the ATLAS detector", *JHEP* **1404** (2014) 169, doi:10.1007/JHEP04(2014)169, arXiv:1402.7029.

[22] ATLAS Collaboration, "Search for the direct production of charginos, neutralinos and staus in final states with at least two hadronically decaying taus and missing transverse momentum in pp collisions at $\sqrt{s}$ = 8 TeV with the ATLAS detector", *JHEP* **1410** (2014) 96, doi:10.1007/JHEP10(2014)096, arXiv:1407.0350.

[23] CMS Collaboration, "The CMS experiment at the CERN LHC", *JINST* **03** (2008) S08004, doi:10.1088/1748-0221/3/08/S08004.

[24] CMS Collaboration, "Commissioning of the Particle-Flow Reconstruction in Minimum-Bias and Jet Events from pp Collisions at 7 TeV", CMS Physics Analysis Summary CMS-PAS-PFT-10-002, 2010.

[25] CMS Collaboration, "Identification of b-quark jets with the CMS experiment", *JINST* **8** (2013) P04013, doi:10.1088/1748-0221/8/04/P04013, arXiv:1211.4462.

[26] CMS Collaboration, "Performance of b tagging at $\sqrt{s} = 8$ TeV in multijet, $\bar{\text{t}}$t and boosted topology events", CMS Physics Analysis Summary CMS-PAS-BTV-13-001, 2013.

[27] CMS Collaboration, "Electron reconstruction and identification at $\sqrt{s} = 7$ TeV", CMS Physics Analysis Summary CMS-PAS-EGM-10-004, 2010.

[28] CMS Collaboration, "Performance of CMS muon reconstruction in pp collision events at $\sqrt{s} = 7$ TeV", *JINST* **7** (2012) P10002, doi:10.1088/1748-0221/7/10/P10002, arXiv:1206.4071.

[29] T. Sjöstrand, S. Mrenna, and P. Skands, "PYTHIA 6.4 physics and manual", *JHEP* **05** (2006) 026, doi:10.1088/1126-6708/2006/05/026, arXiv:hep-ph/0603175.

[30] J. Alwall et al., "MadGraph 5: going beyond", *JHEP* **06** (2011) 128, doi:10.1007/JHEP06(2011)128, arXiv:1106.0522.

[31] GEANT4 Collaboration, "GEANT4—a simulation toolkit", *Nucl. Instrum. Meth. A* **506** (2003) 250, doi:10.1016/S0168-9002(03)01368-8.

[32] CMS Collaboration, "The fast simulation of the CMS detector at LHC", *J. Phys. Conf. Ser.* **331** (2011) 032049, doi:10.1088/1742-6596/331/3/032049.

[33] CMS Collaboration, "Measurement of the Polarization of W Bosons with Large Transverse Momenta in W+Jets Events at the LHC", *Phys. Rev. Lett.* **107** (2011) 021802, doi:10.1103/PhysRevLett.107.021802, arXiv:1104.3829.

[34] ATLAS Collaboration, "Measurement of the polarisation of W bosons produced with large transverse momentum in pp collisions at $\sqrt{s} = 7$ TeV with the ATLAS experiment", *Eur. Phys. J. C* **72** (2012) 2001, doi:10.1140/epjc/s10052-012-2001-6, arXiv:1203.2165.

[35] Z. Bern et al., "Left-Handed W Bosons at the LHC", *Phys. Rev. D* **84** (2011) 034008, doi:10.1103/PhysRevD.84.034008, arXiv:1103.5445.

[36] CMS Collaboration, "Measurement of the properties of a Higgs boson in the four-lepton final state", *Phys.Rev.* **D89** (2014), no. 9, 092007, doi:10.1103/PhysRevD.89.092007, arXiv:1312.5353.

[37] ATLAS Collaboration, "Measurement of Spin Correlation in Top-Antitop Quark Events and Search for Top Squark Pair Production in pp Collisions at $\sqrt{s} = 8$ TeV Using the ATLAS Detector", arXiv:1412.4742.

[38] ATLAS Collaboration, "Measurement of W^+W^- production in pp collisions at $\sqrt{s}$=7 TeV with the ATLAS detector and limits on anomalous WWZ and WWγ couplings", *Phys.Rev.* **D87** (2013), no. 11, 112001, doi:10.1103/PhysRevD.87.112001, 10.1103/PhysRevD.88.079906, arXiv:1210.2979.

[39] CMS Collaboration, "Measurement of W+W- and ZZ production cross sections in pp collisions at sqrt(s) = 8 TeV", *Phys.Lett.* **B721** (2013) 190–211, doi:10.1016/j.physletb.2013.03.027, arXiv:1301.4698.

[40] T. Junk, "Confidence level computation for combining searches with small statistics", *Nucl. Instrum. Meth. A* **434** (1999) 435, doi:10.1016/S0168-9002(99)00498-2, arXiv:hep-ex/9902006.

[41] A. L. Read, "Presentation of search results: the CL_S technique", *J. Phys. G* **28** (2002) 2693, doi:10.1088/0954-3899/28/10/313.

[42] ATLAS and CMS Collaborations, LHC Higgs Combination Group, "Procedure for the LHC Higgs boson search combination in Summer 2011", Technical Report ATL-PHYS-PUB/2011-11, CMS NOTE 2011/005, 2011.

[43] CMS Collaboration, "CMS Luminosity Based on Pixel Cluster Counting - Summer 2013 Update", CMS Physics Analysis Summary CMS-PAS-LUM-13-001, 2013.

[44] S. Alekhin et al., "The PDF4LHC Working Group Interim Report", (2011). arXiv:1101.0536.

[45] M. Botje et al., "The PDF4LHC Working Group Interim Recommendations", (2011). arXiv:1101.0538.

[46] NNPDF Collaboration, "Parton distributions with LHC data", *Nucl. Phys. B* **867** (2013) 244, doi:10.1016/j.nuclphysb.2012.10.003, arXiv:1207.1303.

[47] A. D. Martin, W. J. Stirling, R. S. Thorne, and G. Watt, "Parton distributions for the LHC", *Eur. Phys. J. C* **63** (2009) 189, doi:10.1140/epjc/s10052-009-1072-5, arXiv:0901.0002.

[48] H.-L. Lai et al., "New parton distributions for collider physics", *Phys. Rev. D* **82** (2010) 074024, doi:10.1103/PhysRevD.82.074024, arXiv:1007.2241.

[49] CMS Collaboration, "Search for top-squark pair production in the single-lepton final state in pp collisions at $\sqrt{s}$ = 8 TeV", *Eur .Phys. J. C* **73** (2013) 2677, doi:10.1140/epjc/s10052-013-2677-2, arXiv:1308.1586.

[50] W. Beenakker, R. Höpker, M. Spira, and P. M. Zerwas, "Squark and gluino production at hadron colliders", *Nucl. Phys. B* **492** (1997) 51, doi:10.1016/S0550-3213(97)80027-2, arXiv:hep-ph/9610490.

[51] A. Kulesza and L. Motyka, "Threshold resummation for squark-antisquark and gluino-pair production at the LHC", *Phys. Rev. Lett.* **102** (2009) 111802, doi:10.1103/PhysRevLett.102.111802, arXiv:0807.2405.

[52] A. Kulesza and L. Motyka, "Soft gluon resummation for the production of gluino-gluino and squark-antisquark pairs at the LHC", *Phys. Rev. D* **80** (2009) 095004, doi:10.1103/PhysRevD.80.095004, arXiv:0905.4749.

[53] W. Beenakker et al., "Soft-gluon resummation for squark and gluino hadroproduction", *JHEP* **12** (2009) 041, doi:10.1088/1126-6708/2009/12/041, arXiv:0909.4418.

[54] W. Beenakker et al., "Squark and gluino hadroproduction", *Int. J. Mod. Phys. A* **26** (2011) 2637, doi:10.1142/S0217751X11053560, arXiv:1105.1110.

[55] M. Krämer et al., "Supersymmetry production cross sections in pp collisions at $\sqrt{s}$ = 7 TeV", (2012). arXiv:1206.2892.

[56] B. Fuks, M. Klasen, D. R. Lamprea, and M. Rothering, "Gaugino production in proton-proton collisions at a center-of-mass energy of 8 TeV", *JHEP* **10** (2012) 081, doi:10.1007/JHEP10(2012)081, arXiv:1207.2159.

[57] B. Fuks, M. Klasen, D. R. Lamprea, and M. Rothering, "Precision predictions for electroweak superpartner production at hadron colliders with RESUMMINO", *Eur. Phys. J. C* **73** (2013) 2480, doi:10.1140/epjc/s10052-013-2480-0, arXiv:1304.0790.

[58] B. Fuks, M. Klasen, D. R. Lamprea, and M. Rothering, "Revisiting slepton pair production at the Large Hadron Collider", *JHEP* **01** (2014) 168, doi:10.1007/JHEP01(2014)168, arXiv:1310.2621.